Tribology International 223 (2026) 112233

Contents lists available at ScienceDirect

Tribology International

journal homepage: www.elsevier.com/locate/triboint

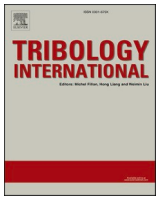

Full length article

Pressure-regulated tribology of a-C/PEEK friction pair under deep-sea environment: Interfacial evolution and atomic-scale simulation

Silong Zhang [a], Xiaowei Li [a,c,*], Peng Guo [a], Xin Zhang [a], Hao Li [a], Rende Chen [a], Zhenyu Wang [a], Kazuhito Nishimura [a], Aiying Wang [a,b,*]

[a] State Key Laboratory of Advanced Marine Materials, Zhejiang Key Laboratory of Extreme-environmental Material Surfaces and Interfaces, Ningbo Institute of Materials Technology and Engineering, Chinese Academy of Sciences, Ningbo 315201, China
[b] Center of Materials Science and Optoelectronics Engineering, University of Chinese Academy of Sciences, Beijing 100049, China
[c] School of Materials Science and Physics, China University of Mining and Technology, Xuzhou 221116, China

ARTICLE INFO

Keywords:
A-C
PEEK
Reactive molecular dynamics
Friction interface
Deep-sea environment

ABSTRACT

Polyetheretherketone (PEEK)/stainless-steel sealing pairs are key components used in the deep-sea environment. However, under high hydrostatic pressure, low temperature, and high salinity, the serious wear and corrosion of the pairs can lead to unpredictable failure. Owing to their excellent wear and corrosion protection properties, amorphous carbon (a-C) coatings have been attempted as a promising solution to this issue. However, limitations in in-situ analysis techniques and high-pressure simulation methods left the atomic-scale evolution of the a-C/PEEK sliding interface poorly understood, leading to a lack of theoretical foundation for designing sealing pairs in a deep-sea environment. In this work, reactive molecular dynamics (RMD) simulations were performed to investigate the pressure-regulated evolution of a-C/PEEK friction interface. Results show that within 1–20 GPa contact pressure range, the friction coefficient first decreases to a minimum of 0.0333 at 5 GPa and then increases, due to the dangling bond passivation and the fluid-to-boundary lubrication transition. The influence of hydrostatic pressure becomes negligible under high contact pressures of at least 5 GPa, while a-C suppresses wear via homogeneous shear. In addition, high pressure promotes seawater ionization, enhancing Cl^-/OH^- adsorption that degrades PEEK's stability by attacking carbonyl groups, which elucidates interfacial failure under mechano-chemical coupling, aiding high-performance deep-sea seal design.

1. Introduction

Mechanical seal components, as the key core parts of deep-sea equipment systems, play a vital role in major deep-sea equipment such as deep-sea oil and gas exploitation equipment, underwater robots, and seabed observation stations [1–3]. In this field, Polyetheretherketone (PEEK) and stainless-steel sealing pairs have been frequently employed, owing to their structural compactness, excellent self-lubricating properties, and cost-effective manufacturability [4–7]. However, under extreme deep-sea service conditions, including high hydrostatic pressure up to 110 MPa, low temperature around 2–4 ℃, and high salinity of seawater [8,9], both serious wear of PEEK and accelerated damage of stainless-steel from corrosion and mechanical wear lead to the inevitable degradation of sealing performance and insufficient long-term stability of equipment [10–12].

Owing to their outstanding physical and chemical properties, including high hardness, low friction coefficient, and excellent corrosion resistance [13–18], amorphous carbon (a-C) coatings have demonstrated significant advantages as an effective strategy for enhancing the service performance of PEEK/stainless-steel pairs for deep-sea equipment. For instance, Franta et al. [19] pointed out that, compared with the uncoated Ti6Al4V alloy, a-C coated counterpart extended the service life from 3×10^5 cycles to 1.98×10^6 cycles, when against PEEK under a 9 g/L NaCl solution. Jacobs et al. [20] applied a-C: W coatings to 100Cr6 bearing steel and on ducted tests against PEEK under both dry and water-lubricated conditions. The wear rate of PEEK was reduced by two orders of magnitude, reaching as low as 10^{-7} $mm^3/(N{\cdot}m)$ under water lubrication. Particularly, Liu et al. [21,22] reported that a-C coatings exhibited excellent protective performance both in high-pressure (60 MPa) simulated deep-sea experiments and a 342-day' deep-sea

* Corresponding authors at: State Key Laboratory of Advanced Marine Materials, Zhejiang Key Laboratory of Extreme-environmental Material Surfaces and Interfaces, Ningbo Institute of Materials Technology and Engineering, Chinese Academy of Sciences, Ningbo 315201, China.
E-mail addresses: xwli@cumt.edu.cn, lixw0826@gmail.com (X. Li), aywang@nimte.ac.cn (A. Wang).

https://doi.org/10.1016/j.triboint.2026.112233
Received 3 March 2026; Received in revised form 20 May 2026; Accepted 23 May 2026
Available online 26 May 2026
0301-679X/

immersion test (5942 m) in the western Pacific.

Although significant progress has been made, a critical challenge still remains, namely, the vast disparity in service environments may lead to dramatically different tribological behavior of a-C/PEEK pairs [23–25]. Especially, in deep-sea environments, it is difficult to extract data through laboratory tests and unravel the coupling effects of multiple environmental factors, such as wear, seawater, and high hydrostatic pressure. And the currently reported high-pressure equipment fails to cover full ocean depth, as it is typically limited to 80 MPa or less [12], not to mention the long testing cycles, high costs, and the general scarcity of resources available for real-sea or equipment-level testing [11]. Relatively, reactive molecular dynamics (RMD) simulations can offer unparalleled atomistic resolution, direct observation of reaction pathways, and have been attempted to unravel the influence of operational conditions. For example, via the RMD method, Li et al. [26] compared the tribological properties of graphene, fullerenes, and carbon nanotubes as oil-based additives at a-C interfaces, revealed evolution of interfacial structure and the interaction between the additives. Liu et al. [27] pointed out that, Coulomb repulsion of CO_2 molecules effectively separated the friction interface, resulting in significantly lower friction coefficient and wear amounts of a-C than those in O_2 environments and dry friction conditions.

Despite efforts, a significant knowledge gap exists regarding the atomic-scale wear mechanisms under the coupled effects of hydrostatic pressure and high contact stress from tribological loading. Especially, the atomic-scale evolution of a-C/PEEK friction interface, including chemical bond breaking and formation, ion adsorption and desorption, interfacial chemical reactions, and the initiation and propagation of internal cracks, remained unclear.

In this work, the RMD simulations were employed to systematically investigate the pressure-regulated evolution of the a-C/PEEK friction interface in a simulated seawater environment. The primary objectives were to specifically decouple the effects of contact pressure (1–20 GPa) from applied tribological loading and ambient hydrostatic pressure (0.11 GPa to simulate full ocean depth), to clarify their individual and synergistic roles on the sliding interface. The resulting atomic-scale insights are expected to provide crucial theoretical guidance for the design of high-performance deep-sea sealing systems.

2. Computational methods

The Large-scale Atomic/Molecular Massively Parallel Simulator (LAMMPS) [28] was employed to carry out all RMD simulations [29]. Fig. 1 shows the schematic diagram of the friction model with a size of $44.79 \times 41.38 \times 170.00$ Å^3 composed of PEEK, a-C, and seawater medium. For the construction process of a-C, 8000 C atoms were deposited on the diamond by an atom-by-atom method [30] to obtain the intrinsic a-C structure, in which the fractions of sp^2- and sp^3-hybridized carbon were 80.10 at% and 16.10 at%, respectively, with a density of 2.61 g/cm^3.(The key parameters for the construction of the a-C model are shown in Fig. S1). Then, 100 H atoms were introduced above the a-C surface following annealing at 600 K with the Nose-Hoover thermostat [31]. After removing unbonded H atoms, 86 H atoms remained chemically adsorbed on the surface. Based on these adsorbed H atoms and 1000 C atoms within the H diffusion depth, the hydrogen content was determined to be 7.92 at%. (Key parameters for the a-C surface hydrogenation process are shown in Fig. S2). For the mated PEEK counterpart, it was constructed with 24 molecular chains, each with a degree of polymerization of 10 [32,33]. The model was then subjected to energy minimization and relaxation to achieve a stable amorphous structure. In addition, 900 H_2O molecules, 10 Na^+ ions, and 10 Cl^- ions were filled into the a-C/PEEK interface to form the seawater medium, corresponding to a 3.5 wt% NaCl concentration.

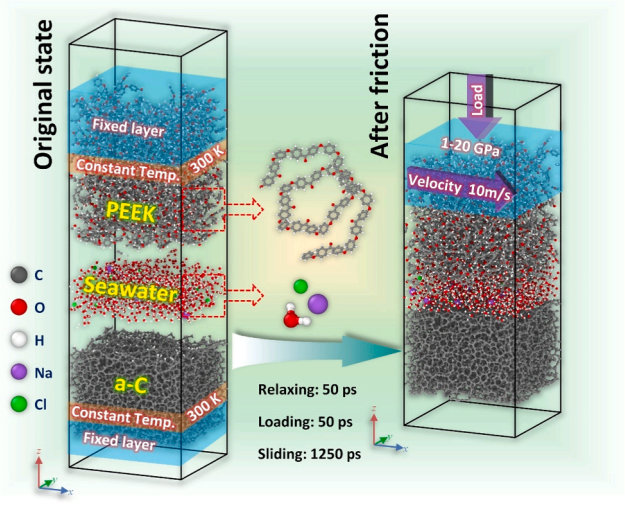

Fig. 1. Schematic diagram of the friction simulation process.

The friction simulation process of a-C/PEEK pairs in seawater environments was shown in Fig. 1. A layered constraint strategy was adopted for the model. Fixed layer: atoms within a 5 Å thickness range at the bottom of the a-C coating and a 20 Å thickness range at the top of the PEEK sealing pair were set as fixed boundaries to restrict the degrees of freedom. Thermostatic layer: atoms within a 10 Å thickness region adjacent to the inner side of the fixed layer (upward from the bottom of the a-C and downward from the top of the PEEK) were maintained at a constant temperature of 300 K using the Berendsen thermostat [34]. Free layer: all atoms except those in the above constrained regions remained in a state of free movement.

Before the friction process, the system was first relaxed at 300 K for 50 ps. Subsequently, an external pressure was applied to the top fixed layer over 50 ps to reach the target values of the preset pressures by the Berendsen barostat algorithm, including the contact pressures of 1, 5, 10, and 20 GPa, as well as the hydrostatic pressure of 0.11 GPa. Although this pressure was much higher than those in experimental conditions, instantaneous contact of amorphous carbon asperities may generate such pressure during friction [35]. Studies by our team [36–38] and other scholars [39–41] have also confirmed that this pressure was suitable for investigating friction behavior at the atomic scale. Due to the short time scale of molecular dynamics calculations and the need for a long sliding distance to achieve effective structural sampling [42–44], a constant velocity of 10 m/s was applied to the top fixed layer along the x-direction, enabling the system to slide under a fixed pressure. The sliding process lasted 1250 ps to reach the steady-state friction stage.

During the friction process, periodic boundary conditions were imposed along the x and y directions, and the time step was set to 0.25 fs. Atomic interactions in the system were described using the Reactive Force Field (ReaxFF) [45]. This force field accounts for instantaneous interatomic interactions via the concept of bond order, permitting the formation and dissociation of covalent bonds as well as chemical reactions in complex carbon-based systems, with a precision comparable to quantum calculations.

3. Results and discussion

To clarify whether the intrinsic hydrostatic pressure of the deep-sea (approximately 0.11 GPa) affects the simulation results, this study systematically analyzed the influence of this hydrostatic pressure on the energy and tribological properties of the a-C/Seawater/PEEK tribological system by comparing pressure conditions differing by 0.11 GPa. Figs. S3 (a)-(d) show the evolution characteristics of the system's kinetic energy (KE), potential energy (PE), pressure, and temperature as a function of friction time before and after the addition of hydrostatic pressure, respectively. Under all simulation conditions, the system successfully reached the preset pressure, verifying the reliability of the

pressure loading protocol; meanwhile, the friction time distribution characteristics of the energy curves were basically consistent. Focusing on the stable friction stage (defined as the final 250 ps of the simulation, the region to the right of the red dashed line in Figs. S3 (a)-(d)), the statistical results in Fig. 2(a) indicate that the impact of the 0.11 GPa hydrostatic pressure on the system's energy state is negligible. Figs. S4 (a)-(d) present the evolution characteristics of the system's friction force and normal force as a function of friction time before and after the addition of hydrostatic pressure, and the friction time distribution characteristics of the friction curves are also basically consistent. Concentrating on the stable friction stage (the region to the right of the red dashed line in Figs. S4 (a)-(d)), the statistical results in Fig. 2(b) show that under pressures of 1 GPa and 1.11 GPa, the 0.11 GPa hydrostatic pressure has a certain effect on the friction force but a minimal impact on the normal force, thereby leading to a decrease in friction coefficient; however, under pressures of 5 GPa and 5.11 GPa, this hydrostatic pressure has negligible impact on either the friction force or the normal force. In summary, the effect of the 0.11 GPa hydrostatic pressure on tribological properties tends to weaken gradually with the increase of applied pressure. Therefore, subsequent analyses will focus on four characteristic pressure points: 1 GPa, 5 GPa, 10 GPa, and 20 GPa.

Figs. S3 (a), (c), (e), and (f) show the evolution of the system's KE, PE, pressure, and temperature as a function of friction time at different contact pressures of 1–20 GPa. Note that during the initial friction stage, the KE and temperature decrease rapidly to stabilize the pressure, with more pronounced reductions observed at higher pressures. Regarding PE evolution, specifically, at 1 GPa and 5 GPa, the PE decreases rapidly in the initial stage, whereas at 10 GPa and 20 GPa, it gradually increases as the sliding processes. Fig. 3(a) summarizes the functional relationships between the system's KE, PE, average temperature, and pressure during the stable friction stage. The data reveals that with increasing pressure, the average KE, PE, and temperature all exhibit an upward trend, accompanied by a simultaneous increase in the fluctuation amplitude of these curves. This phenomenon suggests that the interfacial interactions among the a-C, seawater, and PEEK are enhanced with increasing pressure, thereby promoting the cleavage and formation of chemical bonds within the system [46,47].

Figs. S4 (a), (c), (e), and (f) further depict the evolution of friction force and normal force as a function of friction time. Under all conditions, the a-C/Seawater/PEEK tribological system transitions into the steady state within 1250 ps. The results, summarized in Fig. 3(b), indicate that both the average friction force and normal force increase markedly with pressure from 1 to 20 GPa, accompanied by a rise in the fluctuation amplitude of these forces. The friction coefficient initially decreases and then increases with increasing pressure, reaching a minimum value of 0.0333 at 5 GPa.

Fig. 4 illustrates the interfacial state to clarify the friction behavior of the a-C/seawater/PEEK tribological system. As shown in Fig. 4(a), the number of dangling bonds on the a-C surface decreases with increasing pressure and friction time. These unsaturated surface bonds exhibit high chemical activity. A lower density of dangling bonds decreases the likelihood of a covalent bond with the friction medium and counterpart at the friction interface, thereby lowering the friction coefficient [48,49]. Based on the contact state between a-C and PEEK (Fig. 4(b)), pressure significantly influences the lubrication mechanism. At 1 GPa and 5 GPa, the seawater medium effectively separates the friction pairs, resulting in fluid lubrication. The dangling bonds are progressively passivated through chemical reactions (discussed in detail later), leading to a decline in the friction coefficient, which reaches a minimum at 5 GPa. In contrast, at higher pressures (10 GPa and 20 GPa), the seawater can no longer separate the a-C from the PEEK completely. The number of direct contact points increases with pressure, shifting the lubrication regime from fluid lubrication to boundary lubrication. Under these conditions, increased adhesion and mechanical interlock at the interface outweigh the effect of dangling bond reduction, resulting in an elevated friction coefficient.

To evaluate the wear behavior of the a-C/Seawater/PEEK tribological system under various pressures and analyze the plastic deformation at the atomic scale, the atomic local shear strain (η_i^{Mises}) has been employed as a key characterization parameter [50–53]. This parameter is derived by comparing the current neighbor matrix coordinates (d_{ji}) of an atom with its initial coordinates (d_{ji}^0), and is calculated as follows [54]:

$$\left\{d_{ji}^0\right\} \rightarrow \left\{d_{ji}\right\}, \qquad \forall j \in N_i^0 \tag{1}$$

The transformation matrix J_i is determined by minimizing the

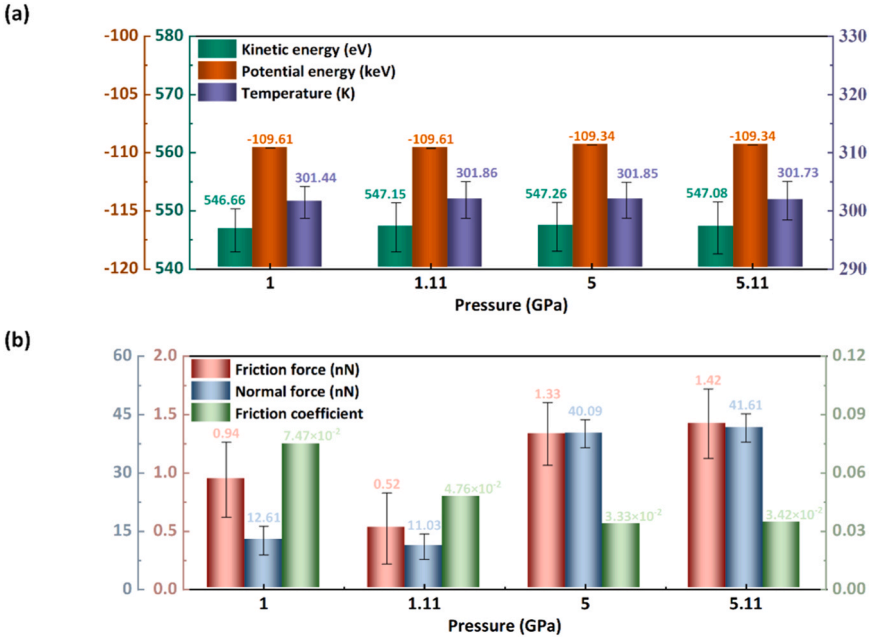

Fig. 2. Relationships among energetic parameters, frictional performance, and pressure before and after the addition of hydrostatic pressure in the a-C/Seawater/PEEK tribological system. (a) energetic parameters; (b) frictional performance. (Error bars denote the standard deviations.).

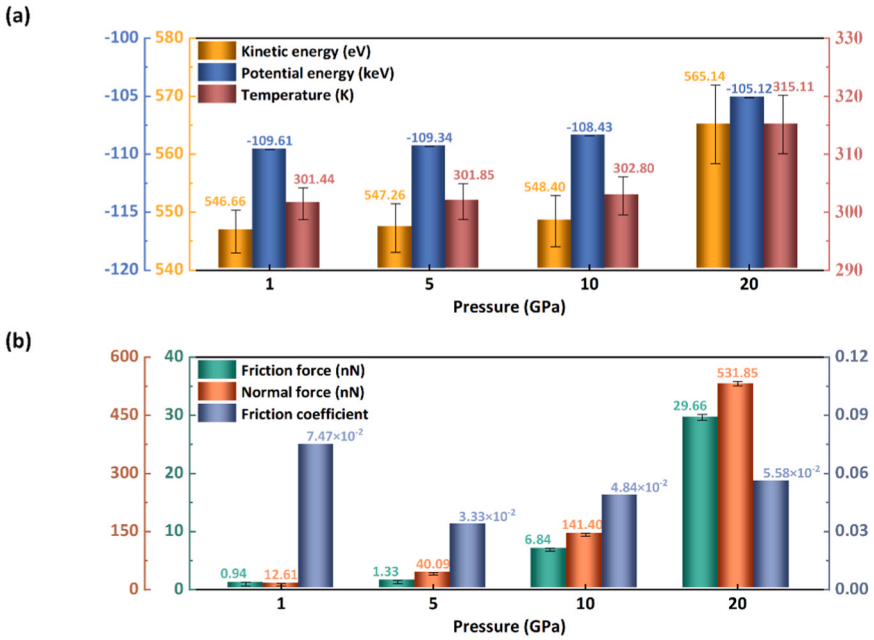

Fig. 3. Relationships among energetic parameters, frictional performance, and pressure without hydrostatic pressure in the a-C/Seawater/PEEK tribological system. (a) energetic parameters; (b) frictional performance. (Error bars denote the standard deviations.).

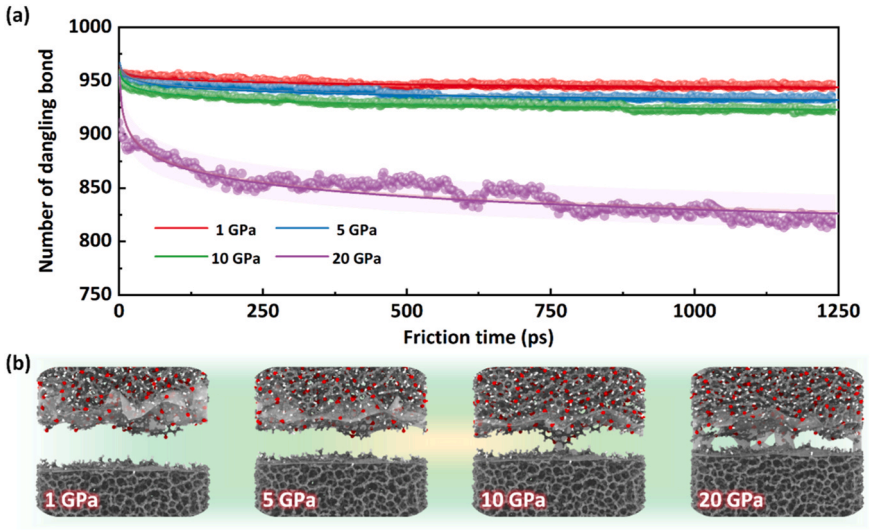

Fig. 4. Analysis of the friction interface state in the a-C/Seawater/PEEK tribological system. (a) Evolution of the dangling bond number on the a-C surface with friction time; (b) Contact state between the a-C and the PEEK.

conversion:

$$\sum_{j\in N_i^0}\left|d_{ji}^0 J_i - d_{ji}\right|^2 = 0 \tag{2}$$

$$J_i = \left(\sum_{j\in N_i^0} d_{ji}^{0T} d_{ji}^0\right)^{-1}\left(\sum_{j\in N_i^0} d_{ji}^{0T} d_{ji}\right) \tag{3}$$

Substitute the transformation matrix J_i into the Green-Lagrange strain tensor formula:

$$\eta_i = \frac{1}{2}\left(J_i J_i^T - I\right) \tag{4}$$

Finally, the local shear strain of the atomiis obtained as:

$$\eta_i^{\text{Mises}} = \sqrt{\eta_{xy}^2 + \eta_{yz}^2 + \eta_{xz}^2 + \frac{\left(\eta_{xx}-\eta_{yy}\right)^2 + \left(\eta_{yy}-\eta_{zz}\right)^2 + \left(\eta_{xx}-\eta_{zz}\right)^2}{6}} \tag{5}$$

Fig. 5(a) present the distribution of shear strain in the a-C/Seawater/PEEK tribological system under various pressures. For clarity, the seawater medium is omitted in these visualizations. At lower pressures (1 GPa and 5 GPa), high shear strain regions (marked in blue) are confined near the interface and exhibit a relatively uniform and ordered distribution, indicating limited shear stress diffusion and mild wear. As pressure increases, these high-strain zones expand markedly into the material interior. Notably, at 20 GPa, the PEEK experiences a sharp increase in the affected area, reflecting enhanced shear disturbance among internal atoms. This intensified strain promotes plastic deformation and microcrack propagation, thereby accelerating wear.

Fig. 5(b) and (c) present the ratios of atoms within different shear

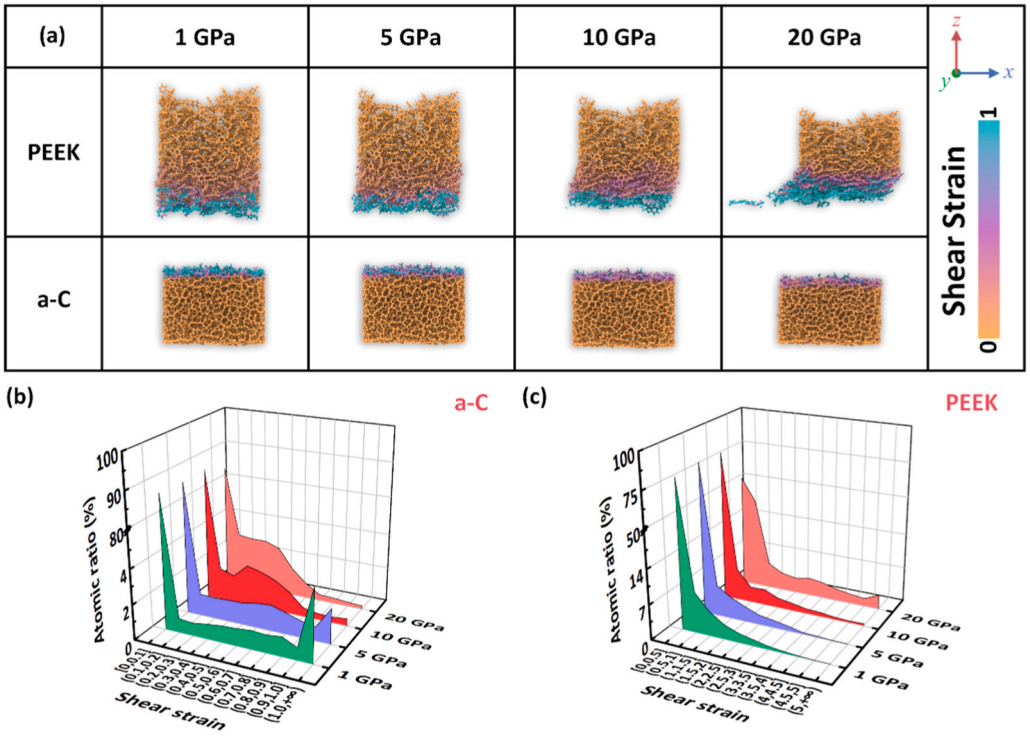

Fig. 5. Influence of pressure on the distribution of local shear strain in the a-C/Seawater/PEEK tribological system. (a) Contour maps of shear strain under various pressures; (b) Distribution of atomic ratios across different shear strain ranges in the a-C; (c) Distribution of atomic ratios across different shear strain ranges in the PEEK.

strain ranges for the a-C and the PEEK, respectively. Atoms in the fixed layer have been excluded from statistics due to boundary constraints

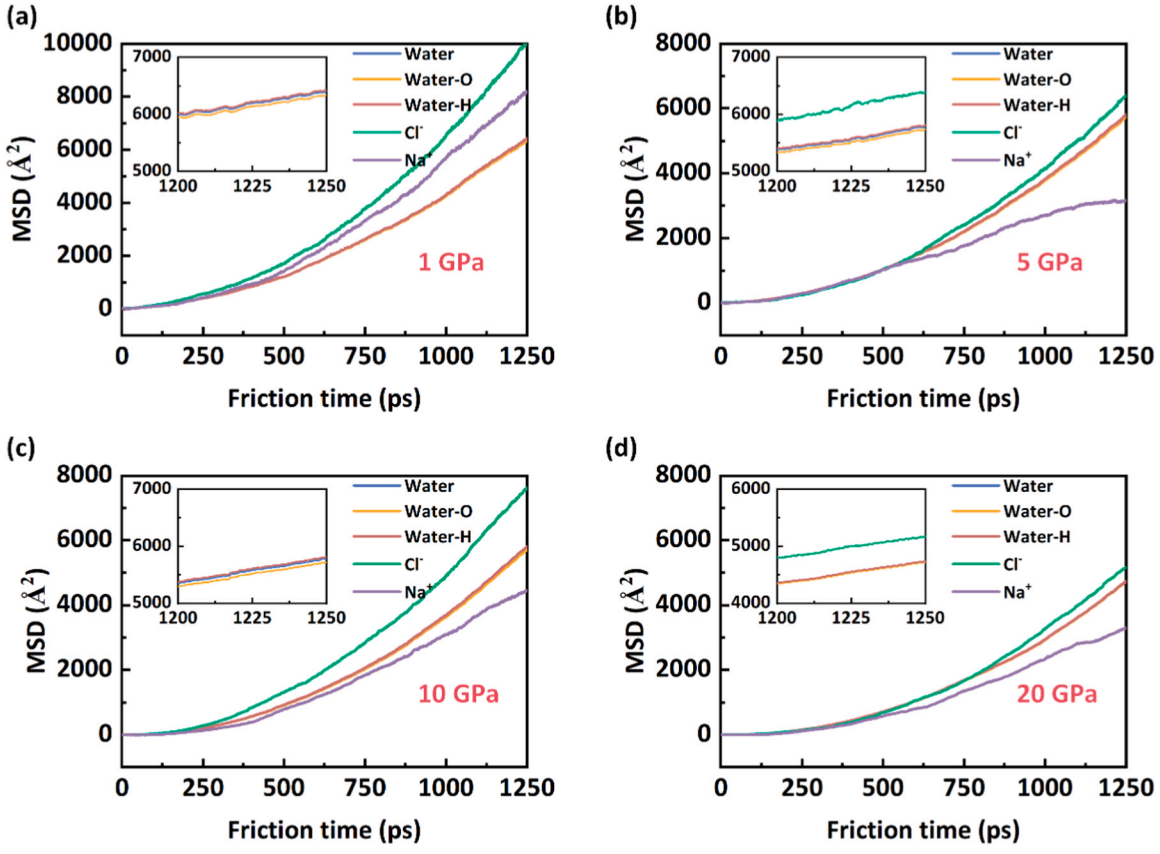

Fig. 6. Evolution of MSD for each component in seawater under various pressures as functions of friction time. (a) 1 GPa; (b) 5 GPa; (c) 10 GPa; (d) 20 GPa.

that prevent relative motion. The shear strain values in PEEK are an order of magnitude higher than those in the a-C, confirming at the atomic-scale that PEEK constitutes the primary wear phase. Specifically, in the a-C, increasing pressure raises the ratios of atoms within the low shear strain range (0.1–0.6), while reducing the ratio in the high strain range (>0.6). This suggests that high pressure promotes shear deformation homogenization, mitigating local strain concentration and thereby enhancing wear resistance. In contrast, due to its lower hardness and elastic modulus, PEEK exhibits a substantial increase in the ratio of high-strain atoms (>3) under high pressure. This reflects intensified strain localization, which facilitates plastic deformation and accelerates wear. The distinct responses of the two materials under pressure highlight the role of their intrinsic properties: the structural stability of a-C promotes uniform strain distribution, while mechanical weakness in PEEK leads to strain concentration. This difference provides a micromechanical basis for the wear behavior of the a-C/Seawater/PEEK tribological system. Regulating pressure to balance interfacial shear deformation uniformity offers a potential pathway for optimizing the tribological performance of this system.

To investigate the structural evolution of the seawater medium during friction in the a-C/Seawater/PEEK tribological system, the mean squared displacement (MSD) has been employed to characterize the mobility of each component [55]. The MSD is defined as:

$$MSD(t) = |r_i(t) - r_i(0)| = \sum_{i=1}^{N} \frac{(dx)^2 + (dy)^2 + (dz)^2}{N} \quad (6)$$

where, $MSD(t)$is the total mean squared displacement of the system at time t; $r_i(t)$ is the position of the i atom at time t; $r_i(0)$ is the position of the i atom at time 0; dx , dy, and dz are the displacement values of the atom in the x, y, and z directions, respectively; $N$is the total number of atoms in the system.

Fig. 6 presents the evolution of MSD for each component in seawater under various pressures as functions of friction time. The results indicate that the Cl^- ions exhibit the highest MSD growth rate across all conditions, reflecting greater mobility compared to other species. This high diffusivity is attributed to their relatively small ionic radius, which facilitates migration within the confined interfacial environment. In contrast, the MSD of Na^+ ions remain comparatively low throughout the sliding process. Among the hydrated components, the hydrogen atoms (Water-H) demonstrate higher diffusivity than the oxygen atoms (Water-O).

This study has investigated the speciation of O and H elements by analyzing the coordination structures of O and H atoms within the seawater medium. Fig. 7 illustrates the evolution of water and its ionization products under various pressures during the friction process. As depicted in Fig. 7(a), the number of H_2O molecules decreases over friction time, with this trend being more pronounced at higher pressures, suggesting that high pressure enhances the ionization of H_2O molecules. Fig. 7(b) shows a gradual increase in OH^- ions, with greater increases under higher pressure, indicating that high-pressure promotes the ionization of H_2O molecules and/or interfacial chemical reactions, leading to increased OH^- generation. Furthermore, as seen in Fig. 7(c), the quantities of both H_3O^+ and H^+ ions rise with time and pressure, further corroborating that high pressure facilitates water ionization.

To further elucidate the interfacial chemical reaction mechanisms during friction, the evolution of bonds formed between H/O atoms in seawater and the a-C or PEEK has been analyzed under various pressures, as shown in Fig. 8. As friction proceeds, the number of O-H bonds in seawater decreases (Fig. 8(a)), with the decline being more pronounced at higher pressures, indicating enhanced ionization of H_2O molecules. The resulting reactive species (OH^- and H^+) participate in subsequent interfacial chemical reactions. Concurrently, the number of

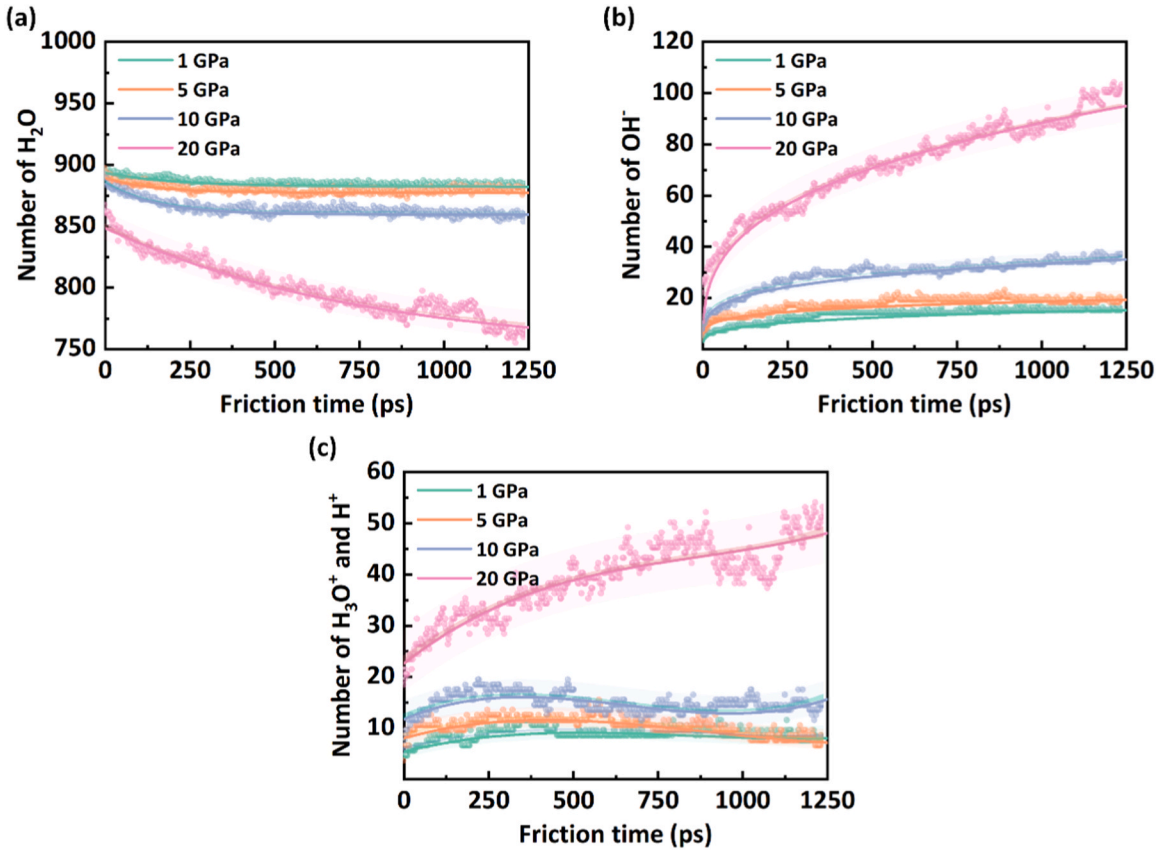

Fig. 7. Evolution of water and its ionization products in seawater medium under various pressures as functions of friction time. (a) H_2O molecules; (b) OH^- ions; (c) H_3O^+ ions and H^+ ions.

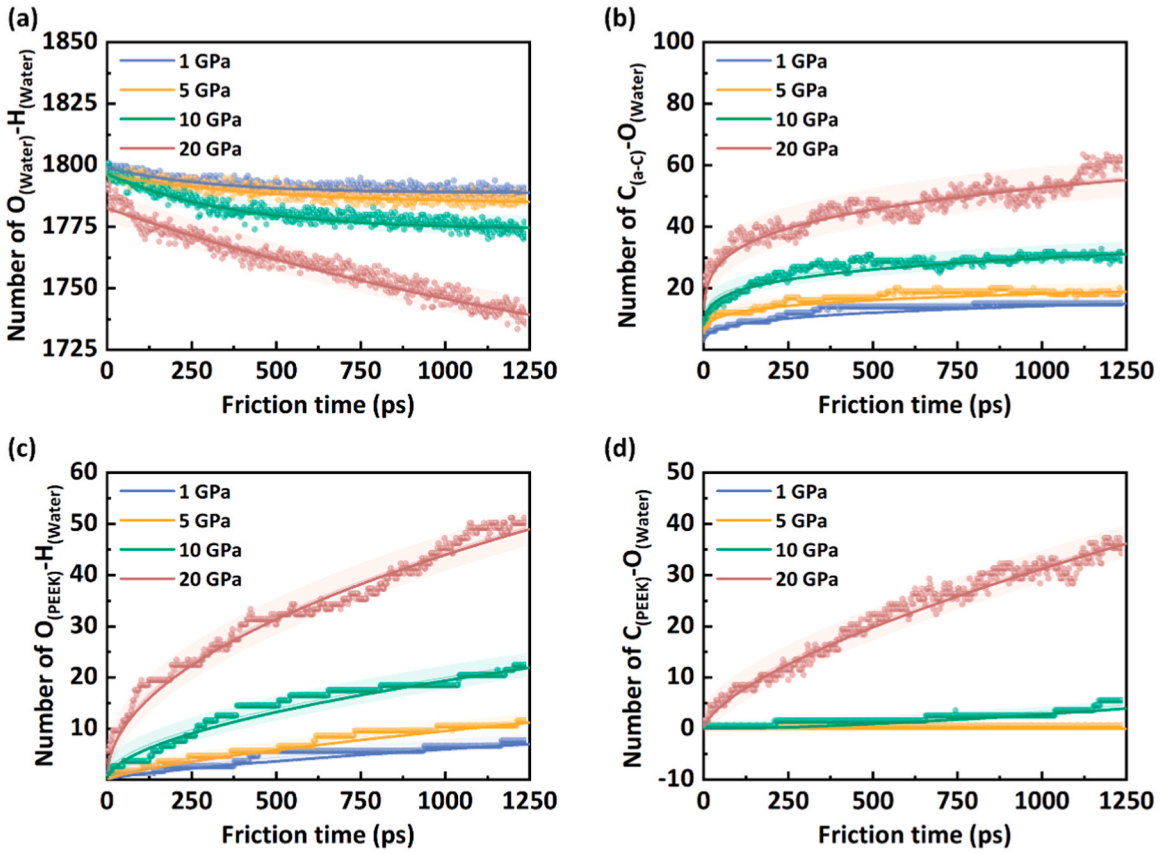

Fig. 8. Evolution of bonds formed between H/O atoms in seawater and the a-C or PEEK under various pressures as functions of friction time. (a) O-H bonds in the seawater; (b) C-O bonds formed between the a-C and the seawater; (c) O-H bonds formed between the PEEK and the seawater; (d) C-O bonds formed between the PEEK and the seawater.

C-O bonds between seawater and the a-C increases over friction time (Fig. 8(b)), exhibiting faster growth and higher final counts under high pressure. Similarly, both O-H and C-O bonds at the PEEK-seawater interface also increase (Fig. 8(c) and (d)), with more significant accumulation under high pressure. These results suggest that high pressure promotes material surface activity and intensifies molecular interactions, facilitating bond cleavage and the formation of new bonds.

Fig. 10 and Fig. S5 present the adsorption and bonding behavior of OH^- and H^+ ions from the seawater medium on the a-C and PEEK under various pressures. Arrows indicate the transition from the initial to the final stage of friction. For clarity, Cl^-, Na^+ ions, and H_2O molecules are omitted. On the a-C surface, the number of adsorbed OH^- ions increases by the end of the friction process, with a notably denser distribution observed at 20 GPa (Fig. 9(a), (b) and Figs. S5 (a), (b)). This suggests that friction combined with high pressure promotes water dissociation, facilitating the adsorption of OH^- ions. Notably, this prominent OH^- adsorption under high pressure is closely coupled to the evolution of carbon hybridization states on the a-C surface. As quantified in the Figs. S6, the friction process induces significant pressure-dependent transformations on the a-C surface: specifically, the ratios of sp-C and sp^2-C decrease most remarkably with increasing pressure and friction time, a trend perfectly consistent with the denser OH^- adsorption distribution at 20 GPa. Importantly, the changes in carbon hybridization directly induced by OH^- adsorption exhibit distinct chemical selectivity. Among all hybridization states, the ratio of sp-C decreases most significantly. This confirms that highly unstable sp-C atoms with abundant dangling bonds serve as the main reaction sites for OH^- ions. This site-specific chemical passivation, realized via the formation of stable C-O bonds, effectively eliminates the most reactive dangling bonds on the a-C surface. These ions passivate the a-C surface by saturating dangling bonds, thereby reducing interfacial interactions and contributing to lower friction.

On the PEEK surface, adsorption of both OH^- and H^+ ions increases after friction. At lower pressures (1 and 5 GPa), H^+ adsorption dominates, while at 10 GPa, significant adsorption of OH^- ions also occur (Fig. 9(c), (d) and Figs. S5 (c), (d)). This indicates a higher adsorption of H element compared to O element species on the PEEK surface. As the primary mobile phase in the tribological system, PEEK contributes to the higher diffusivity of Water-H atoms relative to Water-O atoms, as observed in Fig. 6. To further investigate the bonding mechanisms, the interactions between these ions and functional groups on PEEK were analyzed (Fig. S7). A representative polymer chain has been extracted from PEEK, with C, H, and O atoms in distinct functional groups (e.g., benzene rings, ether bonds, ketone groups) color-coded for clarity (Fig. 9 (e), (f)). The results indicate that after OH^- ions are adsorbed on the PEEK surface, their O atoms mainly form bonds with the C atoms in the ketone groups of PEEK; H^+ ions, when adsorbed on the PEEK surface, mainly form bonds with the O atoms in the ketone groups of PEEK. Apparently, the adsorption of OH^- ions and H^+ ions on the PEEK surface during the friction process will destroy the unsaturated C═O double bonds in the internal ketone groups.

Apart from OH^- ions, Cl^- ions in seawater also act as key corrosive species and were further investigated for their interfacial adsorption and bonding behavior. Fig. 11 and Fig. S8 show the density distributions of Cl^- and Na^+ ions within the seawater medium under various pressures as functions of friction time. The ordinate 0 represents the middle position of the friction model, and the region between the white dashed lines approximates the interface between seawater and the a-C or PEEK. Color intensity represents ion density, with darker red indicating higher concentration. Cl^- ions accumulate prominently near the friction interface,

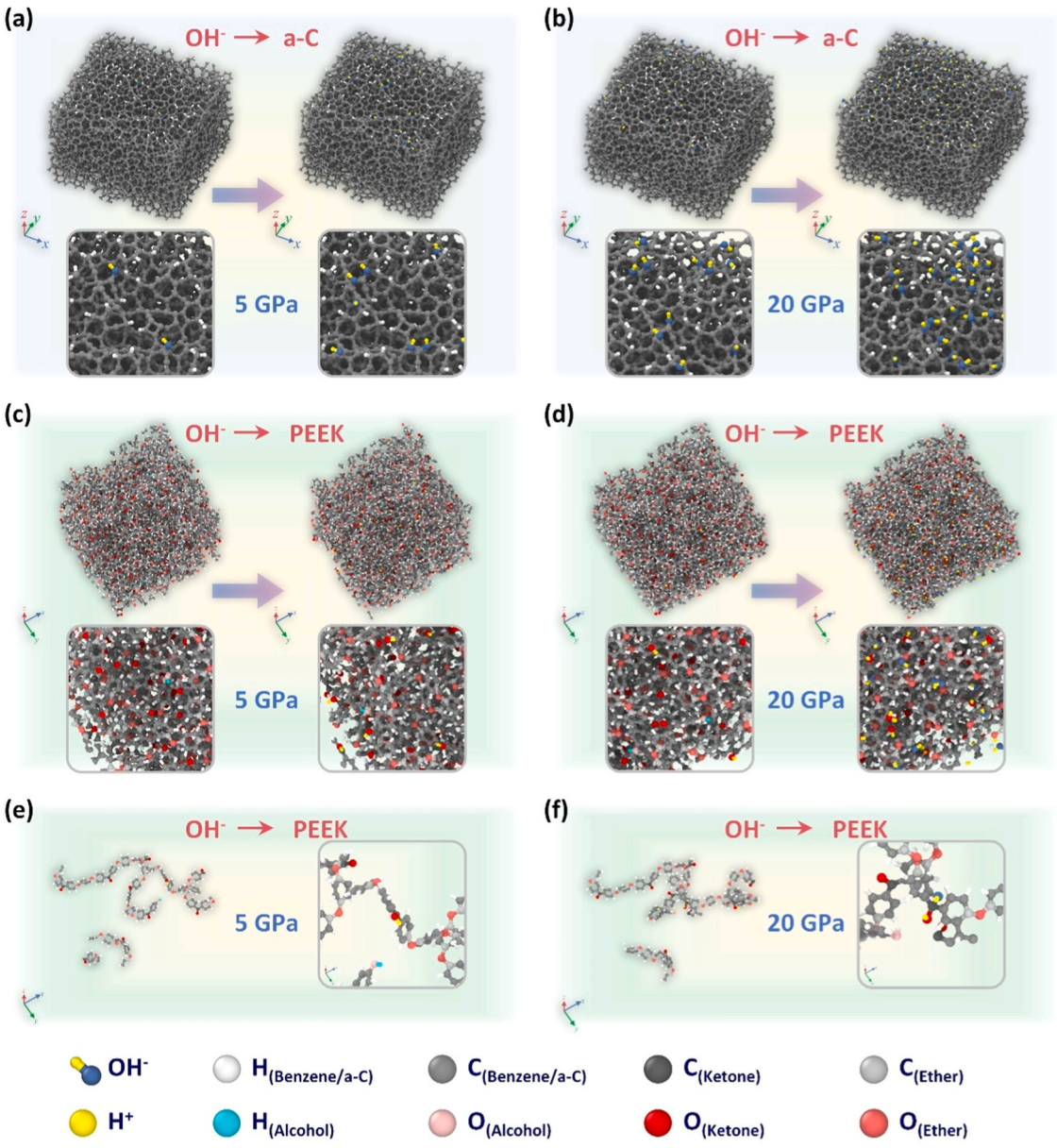

Fig. 9. Adsorption and bonding behavior of OH^- ions and H^+ ions from seawater medium on a-C and PEEK under various pressures. (a), (b) Ions adsorption on the a-C surface; (c), (d) Ions adsorption on the PEEK surface; (e), (f) Bonding behavior between a representative PEEK molecular chain and adsorbed ions at 5 GPa and 20 GPa, respectively.

showing increased density over friction time (Fig. 10 (a), (b) and Figs. S8 (a), (b)). Some Cl^- ions are also observed to diffuse into the PEEK substrate, attributable to its relatively low compactness. This interfacial enrichment enables chemical bonding between Cl^- and the a-C or PEEK, as further supported by the coordination shown in Fig. S9. In contrast, Na^+ ions remain concentrated near the model's middle position rather than accumulating at the friction interface (Fig. 10 (c), (d) and Figs. S8 (c), (d)).

Fig. 11 and Fig. S10 illustrate the adsorption and bonding behavior of Cl^- ions from seawater on the a-C and PEEK under various pressures. Arrows indicate the transition from the initial to the final stage of friction. For clarity, Na^+ ions, H_2O molecules, and ionization products of water are omitted. On the a-C surface, the number of adsorbed Cl^- ions increases after friction, with further enhancement observed at 20 GPa (Fig. 11 (a), (b) and Figs. S10 (a), (b)), indicating that both friction and high-pressure promote Cl^- adsorption. On the PEEK surface, Cl^- adsorption also increases by the end of the friction process. No significant adsorption occurs at 1 GPa or 5 GPa. However, as pressure reaches 10 GPa, clear Cl^- adsorption is observed (Fig. 11 (c), (d) and Figs. S10 (c), (d)), demonstrating that higher pressure facilitates Cl^- binding to PEEK. To elucidate the bonding mechanism, a single polymer chain has been extracted from PEEK, with C, H, and O atoms in distinct functional groups (e.g., benzene rings, ether bonds, ketone groups) color-coded for clarity (Fig. 11 (e)). Analysis reveals that Cl^- ions preferentially form bonds with carbon atoms within the ketone groups, disrupting the unsaturated C═O bonds in PEEK.

4. Conclusions

In this work, RMD simulations were performed to systematically investigate the pressure-regulated interfacial evolution and tribological mechanisms of a-C/PEEK friction pairs under simulated deep-sea environments. Based on the analyses of friction coefficient, wear behavior, and interfacial ion adsorption-reaction processes, the core conclusions

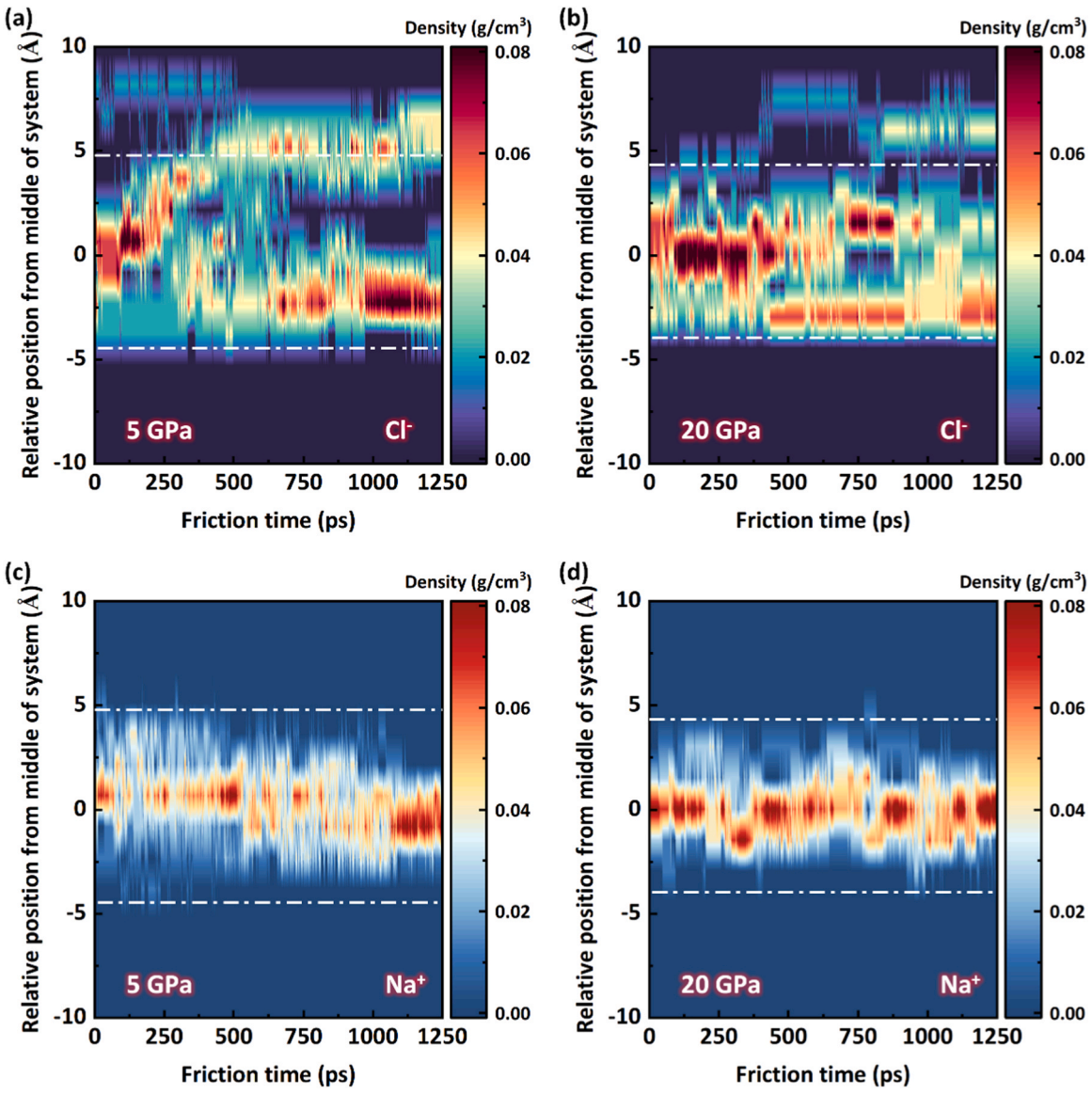

Fig. 10. Density distribution of Cl^- ions and Na^+ ions within the seawater medium under various pressures as functions of friction time. (a), (b) Density distribution of Cl^- ions; (c), (d) Density distribution of Na^+ ions.

are summarized as follows:

(1) The friction coefficient of the a-C/PEEK pair shows a non-monotonic variation with contact pressure (1–20 GPa), reaching a minimum value of 0.0333 at 5 GPa. The deep-sea hydrostatic pressure (0.11 GPa) only slightly affects friction at 1 GPa and becomes negligible at higher contact pressures. The low-friction mechanism is attributed to dangling bond passivation of a-C, while the increase in friction coefficient at high pressure arose from the transition from fluid lubrication to boundary lubrication.

(2) The PEEK is the dominant wear phase under high pressure, whereas the a-C realizes uniform shear distribution and effectively suppresses wear.

(3) High pressure promotes seawater ionization and the enrichment of Cl^-, OH^-, and H^+ at the sliding interface. These ions passivate dangling bonds on a-C to reduce friction, but selectively adsorb at the ketone groups (C═O) of PEEK and break the unsaturated bonds, destabilizing the PEEK structure.

(4) This study reveals the atomic-scale tribological and failure mechanisms of a-C/PEEK pairs in deep-sea environments, providing clear theoretical guidance for material selection, contact pressure matching, and interface modification of deep-sea sealing components, thereby supporting the design of long-life and high-reliability sealing systems for full ocean depth equipment.

CRediT authorship contribution statement

Silong Zhang: Writing – original draft, Validation, Software, Methodology, Investigation, Formal analysis, Conceptualization. **Xiaowei Li:** Writing – review & editing, Software. **Peng Guo:** Writing – review & editing. **Xin Zhang:** Methodology, Investigation. **Hao Li:** Validation. **Rende Chen:** Funding acquisition. **Zhenyu Wang:** Funding acquisition. **Kazuhito Nishimura:** Funding acquisition. **Aiying Wang:** Writing – review & editing, Supervision, Funding acquisition, Conceptualization, Project administration.

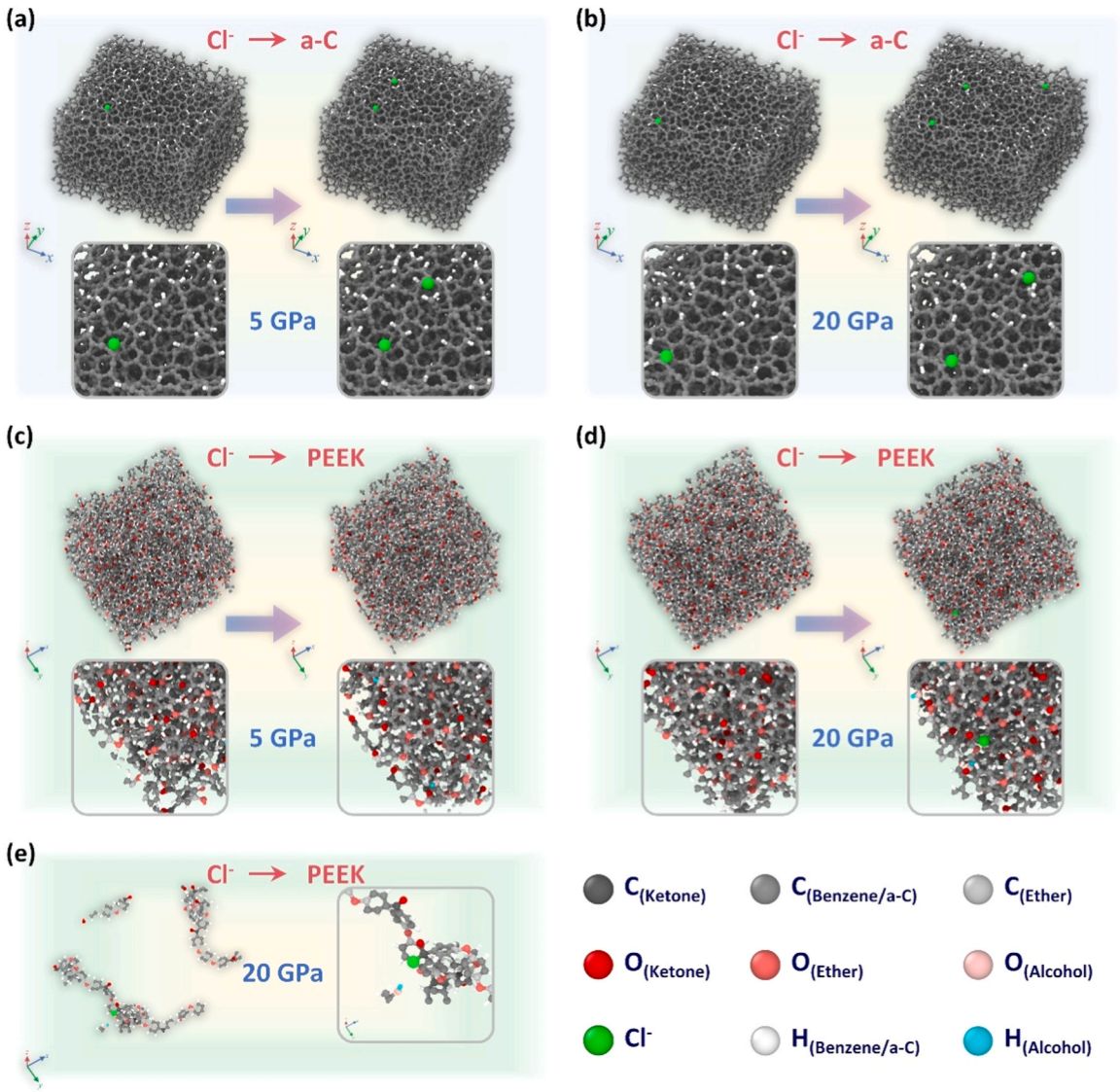

Fig. 11. Adsorption and bonding behavior of Cl^- ions from seawater medium on a-C and PEEK under various pressures. (a), (b) Cl^- ions adsorption on the a-C surface; (c), (d) Cl^- ions adsorption on the PEEK surface; (e) Bonding behavior between a representative PEEK molecular chain and adsorbed Cl^- ions.

Declaration of Competing Interest

The authors declare that they have no known competing financial interests or personal relationships that could have appeared to influence the work reported in this paper.

Acknowledgments

This work was financially supported by the Strategic Priority Research Program of the Chinese Academy of Sciences (XDB1210402), National Natural Science Foundation of China (U24A2030), Zhejiang Lingyan Research and Development Program (2024C01159), Natural Science Foundation of Zhejiang Province (LQN26E050022), Leading Innovative and Entrepreneur Team Introduction Program of Zhejiang (2024R01004), Ningbo Science and Technology 2035 Innovation Project (2024Z134).

Appendix A. Supporting information

Supplementary data associated with this article can be found in the online version at doi:10.1016/j.triboint.2026.112233.

Data Availability

Data will be made available on request.

References

[1] Zhang H, Wang Y, Chen J, Sun Y, Shen Y, Wang H. Research on the reciprocating friction and installation force of seals in deep-sea samplers. Appl Sci 2025;15:1867.
[2] Li Y, Zhao H, Wang D, Xu Y. Metal sealing mechanism and experimental study of the subsea wellhead connector. J Braz Soc Mech Sci Eng 2020;42:26.
[3] Ding X, Wang L, Fan X, Liu X, Zhang Z, Xue B. The synergistic effects of material aging and surface texture on the performance and reliability of marine sealing systems. Ocean Eng 2025;330:121227.
[4] Wang Z, Gao D. Comparative investigation on the tribological behavior of reinforced plastic composite under natural seawater lubrication. Mater Des 2013; 51:983–8.
[5] Guan Z, Wu D, Cheng Q, Wang Z, Tang M, Liu Y. Friction and wear characteristics of CF/PEEK against 431 stainless steel under high hydrostatic pressure water lubrication. Mater Des 2020;196:109057.
[6] Wang Z, Ni J, Gao D. Combined effect of the use of carbon fiber and seawater and the molecular structure on the tribological behavior of polymer materials. Friction 2018;6:183–94.
[7] Zhang Z, Nie S, Yuan S, Liao W. Comparative evaluation of tribological characteristics of CF/PEEK and CF/PTFE/Graphite filled peek sliding against aisi630 steel for seawater hydraulic piston pumps/motors. Tribol T 2015;58: 1096–104.

[8] Yang N, Lv Y, Ji M, Wu S, Zhang Y. High hydrostatic pressure stimulates microbial nitrate reduction in hadal trench sediments under oxic conditions. Nat Commun 2024;15:2473.
[9] Liu H. Synergistic Corrosion Mechanisms of Alloys in High-temperature and high-pressure water environments: A Review. Mater Corros 2025;76:1560–71.
[10] Wu J, Li L. Influence of ambient pressure on sealing performance of O-ring in deep-sea hydraulic system. Ocean Eng 2022;245:110440.
[11] Chen S, Qiu L, Sun S, Yang J, Meng Q, Yang W. Research progress on corrosion of equipment and materials in deep-sea environment. Adv Civ Eng 2021;2021:7803536.
[12] Wu D, Guan Z, Cheng Q, Guo W, Tang M, Liu Y. Development of a friction test apparatus for simulating the ultra-high pressure environment of the deep ocean. Wear 452-453 2020:203294.
[13] Zhou Y, Cui Z, Jiang H, Cao H, Wang D, Yang Q, et al. Achieving robust low friction of diamond-like carbon films in humid air: Exploring the dual effects of doped FeCrNi medium-entropy alloy. Carbon 2024;229:119536.
[14] Zhou Y, Chen Z, Hu Z, Li L, Yang Q, Xing X. Tribological performance of hydrogenated diamond-like carbon coating deposited on superelastic 60NiTi alloy for aviation self-lubricating spherical plain bearings. Chin J Aeronaut 35 2022:309–20.
[15] Lettington A. Applications of diamond-like carbon thin films. Carbon 1998;36:555–60.
[16] Liu Y, Du H, Zuo X, Guo P, Liu L, Lee K, et al. Cr/GLC multilayered coating in simulated deep-sea environment: Corrosion behavior and growth defect evolution. Corros Sci 2021;188:109528.
[17] Wan S, Li D, Zhang G, Tieu A, Zhang B. Comparison of the scuffing behaviour and wear resistance of candidate engineered coatings for automotive piston rings. Tribol Int 2017;106:10–22.
[18] Mustafa M, Umehara N, Tokoroyama T, Murashima M, Shibata A, Utsumi Y, et al. Effect of mesh structure of tetrahedral amorphous carbon (ta-C) coating on friction and wear properties under base-oil lubrication condition. Tribol Int 2020;147:105557.
[19] Franta L, Fojt J, Joska L, Kronek J, Cvrcek L, Vyskocil J, et al. Hinge-type knee prosthesis wear tests with a mechanical load and corrosion properties monitoring. Tribol Int 2013;63:61–5.
[20] Jacobs O, Jaskulka R, Yan C, Wu W. on the effect of counterface material and aqueous environment on the sliding wear of carbon fibre reinforced polyetheretherketone (PEEK). Tribol Lett 2005;19:319–29.
[21] Liu Y, Ma G, Ma X, Li H, Guo P, Wang A, et al. Corrosion and tribocorrosion performance degradation mechanism of multilayered graphite-like carbon (GLC) coatings under deep-sea immersion in the western Pacific. Corros Sci 2024;239:112418.
[22] Liu Y, Zhou X, Guo P, Liu Y, Wei J, Yang W, et al. Effect of hydrostatic pressure on the tribological behavior and mechanism of the multilayered graphite like-carbon (GLC) coating. Friction 2025;13:9440958.
[23] Zhou X, Du N, Li H, Chen R, Lee K, Guo P, et al. Oxygen-related interfacial tribo-chemical reaction and wear mechanism between a-C coating and PEEK. Tribol Int 2025;211:110840.
[24] Zhou X, Zhang Y, Li H, Cui L, Yang W, Wang A, et al. Cr doping modification for tribological behavior of Cr/a-C multilayer coatings against PEEK under diverse operational conditions. Friction 2025;13:9440920.
[25] Zhou X, Zhang Y, Guo P, Cui L, Wang A, Ke P. Tribological behavior of Cr/a-C multilayered coating against PEEK under dry sliding condition. Wear 2023:518–9.204625.
[26] Li X, Xu X, Zhou Y, Lee K, Wang A. Insights into friction dependence of carbon nanoparticles as oil-based lubricant additive at amorphous carbon interface. Carbon 2019;150:465–74.
[27] Liu Y, Xu P, Zhu X, Luo Y, Zhang H, Wang X, et al. Interfacial friction evolution of DLC films on the fracturing pump plungers during the CO_2 fracturing process: An atomic understanding from reaxff simulations. Tribol Lett 2023;71:126.
[28] Plimpton S. Fast parallel algorithms for short-range molecular dynamics. J Comput Phys 1995;117:1–19.
[29] Van Duin A, Dasgupta S, Lorant F, Goddard W. ReaxFF: A reactive force field for hydrocarbons. J Phys Chem A 2001;105:9396–409.
[30] Li X, Wang A, Lee K. Comparison of empirical potentials for calculating structural properties of amorphous carbon films by molecular dynamics simulation. Comp Mater Sci 2018;151:246–54.
[31] Evans D, Holian B. The Nose-Hoover thermostat. J Chem Phy 1985;83:4069–74.
[32] Wang Y, Chen J, Tang H, Yang B, Wang S, Wang N. Molecular dynamics simulation and experimental study on the mechanical properties of functionalized graphene-enhanced PEEK/PTFE. Polymers 2025;18:125.
[33] Qi Y, Sun B, Zhang Y, Gao G, Zhang P, Zheng X. Tribological properties of nano-ZrO_2 and PEEK reinforced PTFE composites based on molecular dynamics. Lubricants 2023;11:194.
[34] Berendsen H, Postma J, van Gunsteren W, DiNola A, Haak JR. Molecular dynamics with coupling to an external bath. J Chem Phy 1984;81:3684–90.
[35] Ma T, Wang L, Hu Y, Li X, Wang H. A shear localization mechanism for lubricity of amorphous carbon materials. Sci Rep 2014;4:3662.
[36] Li X, Wang A, Lee K. Mechanism of contact pressure-induced friction at the amorphous carbon/alpha olefin interface. Npj Comput Mater 2018;4:53.
[37] Li X, Wang A, Lee K. Insights on low-friction mechanism of amorphous carbon films from reactive molecular dynamics study. Tribol Int 2019;131:567–78.
[38] Li X, Wang A, Lee K. Tribo-induced structural transformation and lubricant dissociation at amorphous carbon-alpha olefin interface. Adv Theor Simul 2019;2:1800157.
[39] Ma T, Hu Y, Wang H. Molecular dynamics simulation of shear-induced graphitization of amorphous carbon films. Carbon 2009;47:1953–7.
[40] Kuwahara T, Romero P, Makowski S, Weihnacht V, Moras G, Moseler M. Mechano-chemical decomposition of organic friction modifiers with multiple reactive centres induces superlubricity of ta-C. Nat Commun 2019;10:151.
[41] Bai S, Murabayashi H, Kobayashi Y, Higuchi Y, Ozawa N, Adachi K, et al. Tight-binding quantum chemical molecular dynamics simulations of the low friction mechanism of fluorine-terminated diamond-like carbon films. RSC Adv 2014;4:33739.
[42] Bai S, Onodera T, Nagumo R, Miura R, Suzuki A, Tsuboi H, et al. Friction reduction mechanism of hydrogen- and fluorine-terminated diamond-like carbon films investigated by molecular dynamics and quantum chemical calculation. J Phys Chem C 2012;116:12559–65.
[43] Wang Y, Xu J, Ootani Y, Bai S, Higuchi Y, Ozawa N, et al. Tight-binding quantum chemical molecular dynamics study on the friction and wear processes of diamond-like carbon coatings: Effect of Tensile Stress. ACS Appl Mater Interfaces 2017;9:34396–404.
[44] Wang Y, Xu J, Zhang J, Chen Q, Ootani Y, Higuchi Y, et al. Tribochemical reactions and graphitization of diamond-like carbon against alumina give volcano-type temperature dependence of friction coefficients: A tight-binding quantum chemical molecular dynamics simulation. Carbon 2018;133:350–7.
[45] Tavazza F, Senftle T, Zou C, Becker C, Van Duin A. Molecular dynamics investigation of the effects of tip-substrate interactions during nanoindentation. J Phys Chem C 2015;119:13580–9.
[46] Sun Y, Wang G, Cheng Q, Li J, Yin T, Wang B. Molecular dynamics investigation of the nanoindentation performance of PTFE reinforced with DLC coatings. Diam Relat Mater 2025;158:112633.
[47] Zhao G, Yin T, Song J, Wang G, Xue F, Ding Q. Continuous heat generation during polymer friction: aperiodic conformational fluctuations of molecular chains. ACS Appl Polym Mater 2025;7:13471–7.
[48] Derry T, Madiba C, Sellschop J. Oxygen and hydrogen on the surface of diamond. Nucl Instrum Meth B 1983;218:559–62.
[49] Su C, Lin J. Thermal desorption of hydrogen from the diamond C(100) surface. Surf Sci 1998;406:149–66.
[50] Chen J, Liu C, Liu H, Zhang B, To S. Atomic insight into the speed effect on deformation mechanisms in nano-scratching of monocrystalline iron. Precis Eng 2025;92:219–30.
[51] Liu Y, Zhang H, Liu T, Wang X, Luo Y, Zhu X. Exploring the effects of water content on friction behavior and mechanism of DLC films in oil production environment based on molecular dynamics simulation and first-principles calculations. Diam Relat Mater 2023;139:110294.
[52] Huang G, Chen O, Cheng Q, Yin T, Ren K, Ma C, et al. Interfacial ice layer mediates anti-wear of PEEK during cryogenic sliding: An atomic-scale insight. Appl Surf Sci 2026;724:165685.
[53] Wang G, Cheng Q, Yin T, Zhang Y, Ma C, Zhao G. Vibration-induced dynamic interfacial adjustment of PTFE friction in an aqueous environment from the nanoscale. Tribol Int 2025;212:111015.
[54] Shimizu F, Ogata S, Li J. Theory of shear banding in metallic glasses and molecular dynamics calculations. Mater Trans 2007;48:2923–7.
[55] Zhang J, Yang J, Hou D, Ding Q. Molecular dynamics study on calcium aluminosilicate hydrate at elevated temperatures: Structure, dynamics and mechanical properties. Mater Chem Phys 2019;233:276–87.